

# High Excitation Molecular Gas in the Magellanic Clouds

Alberto D. Bolatto

*Department of Astronomy & Radio Astronomy Laboratory*

*University of California at Berkeley,  
601 Campbell Hall, Berkeley, CA 94720-3411, USA*

`bolatto@astro.berkeley.edu`

Frank P. Israel

*Sterrewacht Leiden, Leiden University*

*P.O. Box 9513, NL 2300-RA Leiden, The Netherlands*

`israel@strw.leidenuniv.nl`

and

Christopher L. Martin

*Department of Physics and Astronomy*

*Oberlin College, Wright Laboratory of Physics,  
110 North Professor Street, Oberlin, Ohio 44074-1088 USA*

`Chris.Martin@oberlin.edu`

## ABSTRACT

We present the first survey of submillimeter  $^{12}\text{CO}$  ( $J = 4 \rightarrow 3$ ) emission in the Magellanic Clouds. The survey is comprised of 15  $6' \times 6'$  maps obtained using the AST/RO telescope toward the molecular peaks of the Large and Small Magellanic Clouds. We have used these data to constrain the physical conditions in these objects, in particular their molecular gas density and temperature. We find that there are significant amounts of molecular gas associated with most of these molecular peaks, and that high molecular gas temperatures are pervasive throughout our sample. We discuss whether this may be due to the low metallicities and the associated dearth of gas coolants in the Clouds, and conclude that the present sample is insufficient to assert this effect.

*Subject headings:* Magellanic Clouds — galaxies: ISM — submillimeter

## 1. Introduction

With their proximity, their unextinguished lines of sight, and their profuse star formation, the Magellanic Clouds are some of the best extragalactic objects in which to study the relationship between molecules and star formation. Because the interstellar medium (ISM) in the Magellanic Clouds is deficient in heavy elements and dust, molecular observations of these objects probe an interesting regime, perhaps more similar to the conditions in early protogalaxies rather than those prevalent today in the Milky Way. Indeed, studies of active, metal-poor, nearby dwarf galaxies such as the Magellanic Clouds should offer insight into the processes at work in primeval sources.

What are the effects of low metallicities on the star-forming molecular ISM? We know that molecules are more difficult to form both in the gas phase (less O, C, and N) and on grain surfaces (fewer grains), and that they are easier to destroy (diminished dust shielding of the UV radiation) in low metallicity environments. Thus, molecules other than H<sub>2</sub> are more rare in these sources which in particular translates into a dearth of CO emission in the Magellanic Clouds and other dwarf irregulars (e.g., Israel et al., 1986; Israel, Tacconi & Baas 1995, Taylor, Kobulnicky, & Skillman 1998; Leroy et al. 2005). Furthermore, because the FIR and submillimeter lines of the different forms of carbon and oxygen (C<sup>+</sup>, C, O, and CO) dominate the cooling of the star-forming ISM (e.g., Le Bourlot et al. 1993; Wolfire et al. 1995), the lower abundances of these elements will make the cooling of the molecular gas less efficient. However, at the same time smaller dust-to-gas ratios will yield lower heating of the molecular gas, as photoelectric ejection of electrons from small dust grains is the chief mode by which starlight heats the gas phase of the ISM. If molecular gas temperatures were considerably affected by the metallicity of the ISM, we expect important consequences for star formation in such environments. In particular, if the Jeans criterion is relevant to star-formation, the mass of collapsible clouds grows for decreasing metallicity as the Jeans mass increases  $M_J \sim T^{3/2}$ . Such change could have important effects on the Initial Mass Function of stars in these systems. To a first approximation, models suggest that lowering the metallicity causes a similar decrement in both heating (by diminishing the dust-to-gas ratio) and cooling (by diminishing the C and O abundances; Wolfire et al. 1995).

It is important to realize, however, that there are many possibilities likely to complicate this simple picture. For example, if the dust-to-gas ratio were to decrease faster than the metallicity (as suggested by Lisenfeld & Ferrara 1998), or if there were a lack of very small dust grains in the low metallicity ISM (as suggested by the faintness of the polycyclic aromatic hydrocarbon emission observed toward some of these sources; e.g., Madden 2000), the heating processes may become less efficient and the balance may be shifted toward lower temperatures. Furthermore, because it is also necessary to consider the metallicity threshold

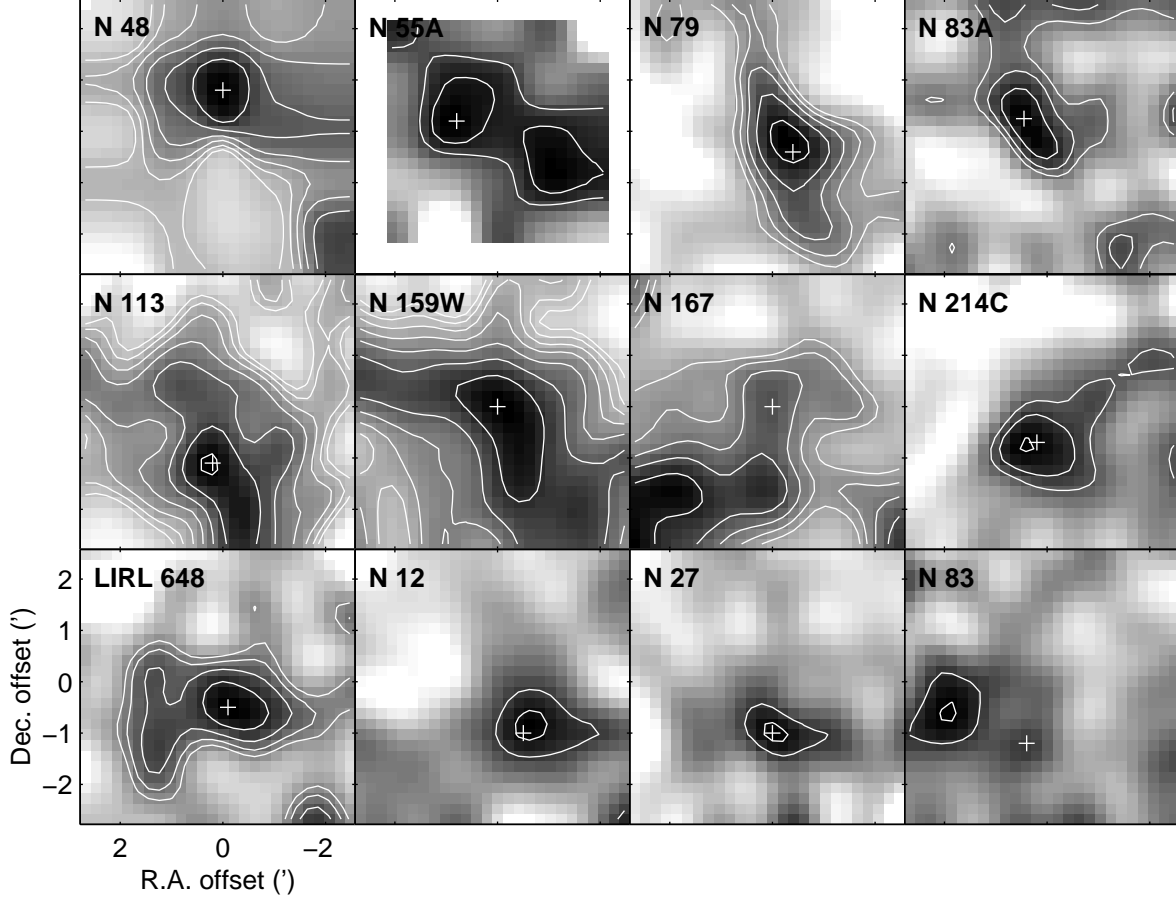


Fig. 1.—  $^{12}\text{CO}$  ( $J = 4 \rightarrow 3$ ) maps obtained toward our detected sources in the LMC/SMC. The coordinates of the central positions of the maps (offsets 0,0) are listed in Table 1. The contours are logarithmically spaced, starting at  $1.5 \text{ K km s}^{-1}$  and increasing by factors of 1.3 (except for N 79, N 83A, N 113, and N 159W, where they start at  $2.5 \text{ K km s}^{-1}$ ). These maps were produced by convolving the data with a Gaussian of  $\text{FWHM}=1'$ . Most maps are sampled on a  $30''$  grid, except for N 48 and N 55A where the grid spacing used was  $60''$ . The positions marked by the crosses are those of the  $\text{CO}$  ( $J = 1 \rightarrow 0$ ) sources, where we measured the intensities used in the LVG analysis.

below which hitherto secondary heat sources (e.g., chemical heating) become important, the effects of metallicity on the heating and cooling balance of molecular clouds are very difficult to address from a purely theoretical approach.

Answering some of these questions observationally requires studying the physical conditions of the molecular gas in nearby, low metallicity sources. At distances of 55 and 63 kpc, the proximity of the Magellanic Clouds affords single-dish millimeter-wave observations excellent spatial resolution attainable in other galaxies only through the use of interferometers, which permits detailed studies of individual clouds instead of ensemble properties. In particular, the ability to spatially separate the emission from different regions makes the Magellanic Clouds ideal targets to study the excitation of the molecular gas and its relationship with star formation. Multitransition studies of CO and other molecules are very useful tools to determine the physical conditions of the H<sub>2</sub> (e.g., Johansson et al. 1998; Heikkilä 1998; Chin et al. 1998; Heikkilä et al. 1999), but their application is limited if there is no information on the intensities of the higher CO transitions, which are extremely sensitive to density and temperature. Because of their southern declination, however, there is a dearth of submillimeter observations of the Clouds.

We present here a survey of <sup>12</sup>CO ( $J = 4 \rightarrow 3$ ) in the molecular peaks of the Magellanic Clouds, and the results of an excitation analysis using these and lower  $J$  observations. These pointings were selected among the brightest <sup>12</sup>CO ( $J = 1 \rightarrow 0$ ) peaks found by SEST observations (Israel et al. 1993), many of which are associated with star-forming complexes and Henize (1956) H $\alpha$  nebulosities, and are thus denoted using the corresponding “N” number. In section §2 we present the observations, in §3 we discuss the LVG analysis and its results, and in §4 we summarize our conclusions.

## 2. Observations and Results

We observed the ( $J = 4 \rightarrow 3$ ) transition of carbon monoxide (<sup>12</sup>CO) at  $\nu \simeq 461.0408$  GHz (650.7  $\mu$ m) using AST/RO, the Antarctic Submillimeter Telescope and Remote Observatory located at the Amundsen–Scott South Pole base (Stark et al. 2001). The observations were obtained on the austral winter of 2002, using the lower frequency side of the dual AST/RO SIS waveguide receiver (Walker et al. 1992; Honingh et al. 1997), with system temperatures of  $T_{sys} \sim 2000$  K. The backend was the 2048 channel low resolution (1.07 MHz resolution, 0.68 MHz channels) acousto-optical spectrometer (Schieder, Tolls, and Winnemisser 1989). The spectra were observed in position switching mode, chopping 25' in Azimuth (which is the same as R.A. at the pole). At 461 GHz, the telescope beam was measured to have a HPBW  $\approx 109''$ . The forward efficiency determined from skydips was

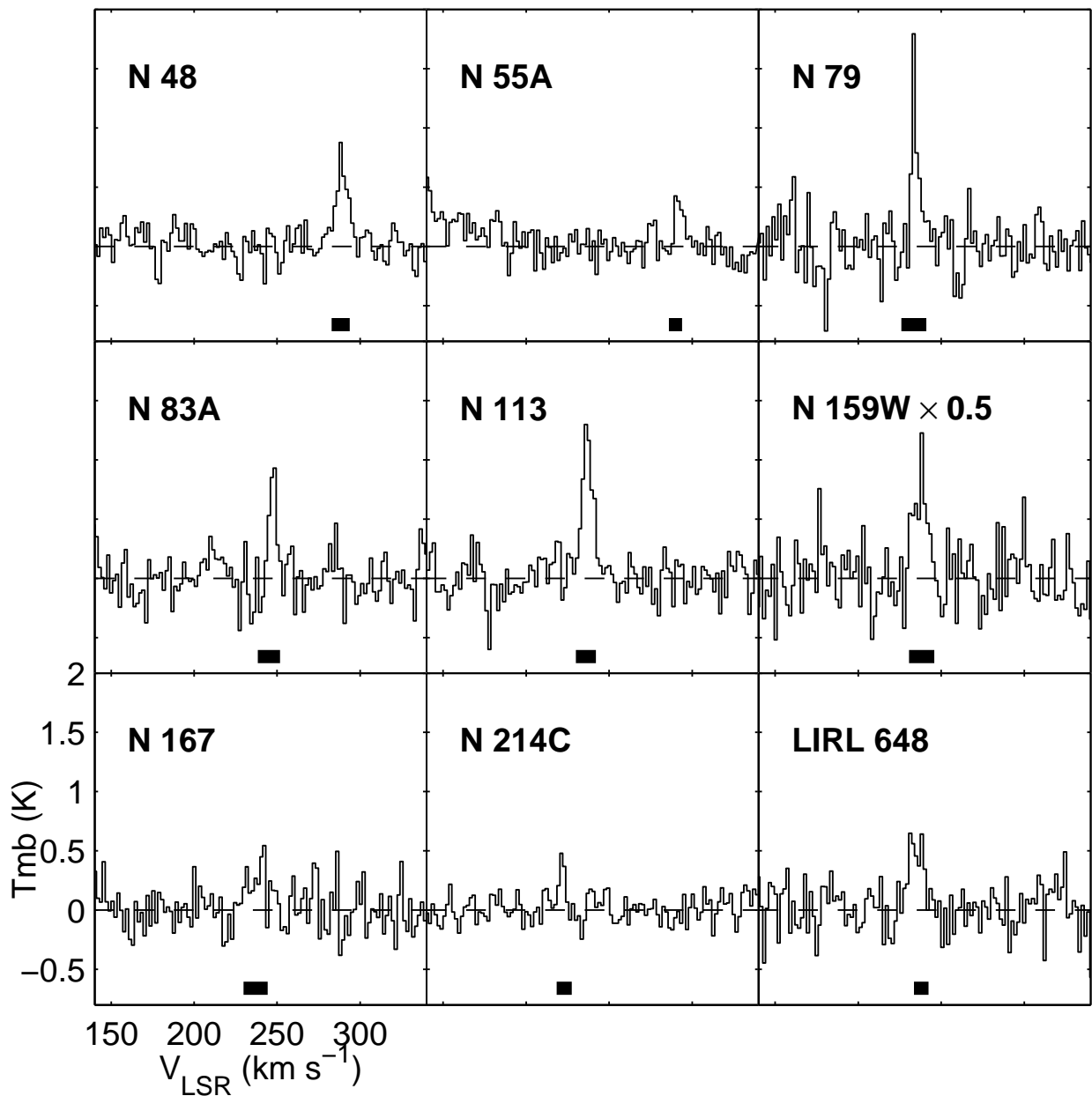


Fig. 2.— Spectra of  $^{12}\text{CO}$  ( $J = 4 \rightarrow 3$ ) emission in LMC sources. These spectra were obtained toward the positions marked by crosses in Fig. 1. All sources were detected. The emission in N 159W is shown scaled down by a factor of two for display purposes. The thick black line near the bottom of the plots indicates the velocity and width of the CO emission in the lower  $J$  transitions, as observed using SEST.

$\sim 70\%$ , and is assumed to be identical to  $\eta_{mb}$ . Maps of size  $6' \times 6'$  centered on the SEST coordinates (c.f. Table 1) were obtained for each region, using a  $30''$  grid (in a few cases the maps were done on a  $60''$  grid). The data were calibrated using the standard procedure for AST/RO, which includes sky, ambient and cold load measurements every 20–30 minutes, and processed using the COMB astronomical package. The individual maps are shown in Fig. 1, and representative spectra are shown in Figs. 2 and 3. Because the pointing accuracy is estimated to be  $\sim 1'$ , we have selected the emission peaks closest to the center of the map within those margins to measure the integrated intensities compiled in Table 1 (indicated by the crosses in Fig. 1). Note that this method may introduce a bias in the direction of obtaining larger CO ( $J = 4 \rightarrow 3$ )/( $J = 1 \rightarrow 0$ ) ratios. Nonetheless we feel that this methodology is justified, as in the Milky Way the positional coincidence between the peaks of both transitions is very often observed. In some cases it is apparent that the structure of the sources is complex (e.g., N 159W; Bolatto et al. 2000), and in particular for N 167 and N 83 the brightest emission peak is well away from the central position. Given the large and variable effects of the atmosphere at submillimeter wavelengths and the pointing accuracy of the telescope, we estimate the overall absolute calibration accuracy of the data to be  $\sim 30\%$ .

Table 1 summarizes our observations. Column 4 lists the  $^{12}\text{CO}$  ( $J = 1 \rightarrow 0$ ) integrated intensities observed by the SEST Magellanic Cloud Key Programme toward our sources, while column 5 shows the intensities convolved to the angular resolution of AST/RO. Finally, column 6 lists the  $^{12}\text{CO}$  ( $J = 4 \rightarrow 3$ ) integrated intensities used in our LVG analysis, with their statistical errors. These intensities are those measured in the AST/RO pointings marked with crosses in Fig. 1.

### 3. Analysis and Discussion

#### 3.1. Modeling of CO

The available observed  $^{12}\text{CO}$  and  $^{13}\text{CO}$  line ratios have been modelled using the large-velocity gradient (LVG) radiative transfer models described by Jansen (1995) and Jansen et al. (1994). These models provide line intensities as a function of three input parameters: gas kinetic temperature  $T_k$ , molecular hydrogen density  $n(H_2)$  and CO column density per unit velocity ( $N(\text{CO})/dV$ ). By comparing model line *ratios* to the observed ratios we

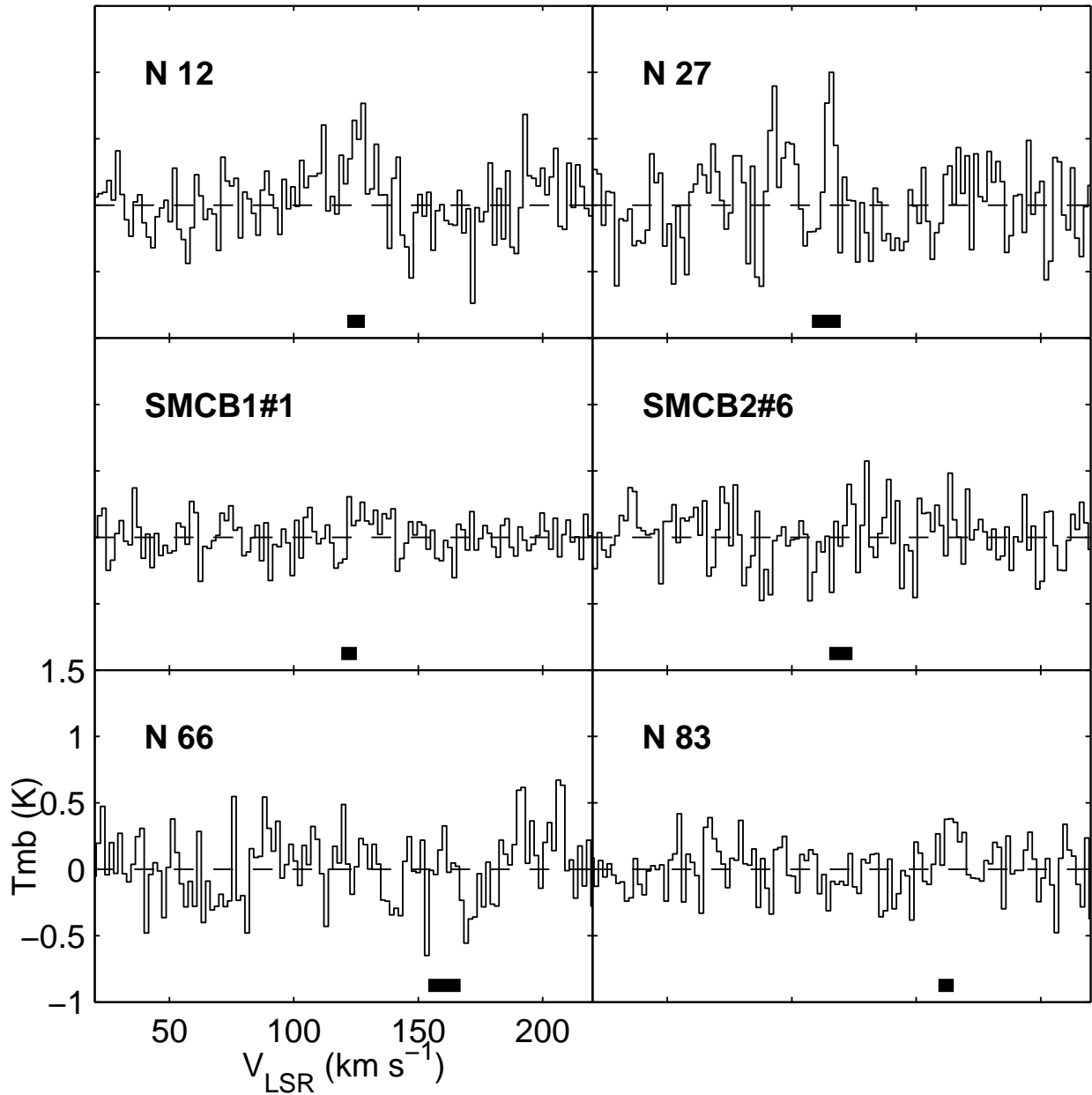


Fig. 3.— Spectra of  $^{12}\text{CO}$  ( $J = 4 \rightarrow 3$ ) emission in SMC sources, obtained toward the positions marked with crosses in Fig. 1. Only N 12, N 27, and N 83 were detected, and the signals are in general considerably weaker than in the LMC. As in the previous figure, the  $\text{CO}$  ( $J = 1 \rightarrow 0$ ) velocity and linewidth are indicated by the thick black line at the bottom of the plots.

Table 1. AST/RO and SEST CO observations of Magellanic cloud H II regions

Source	Coordinates		Observed $^{12}\text{CO}$ Integrated Intensities in $\text{K km s}^{-1}$		
	R.A. (B1950)	Dec. (B1950)	(43'') ( $J = 1 \rightarrow 0$ )	(109'') ( $J = 1 \rightarrow 0$ )	(109'') ( $J = 4 \rightarrow 3$ )
<b>LMC</b>					
N 48	05 <sup>h</sup> 25 <sup>m</sup> 46 <sup>s</sup> .6	−66°17′36''	3.7	...	6.6±0.7
N 55A	05 <sup>h</sup> 32 <sup>m</sup> 30 <sup>s</sup> .0	−66°29′21''	17.4	4.9	2.5±0.5
N 79	04 <sup>h</sup> 52 <sup>m</sup> 09 <sup>s</sup> .5	−69°28′21''	21.3	...	6.0±0.7
N 83A	04 <sup>h</sup> 54 <sup>m</sup> 17 <sup>s</sup> .0	−69°16′23''	21.1	6.6	10.4±1.4
N 113	05 <sup>h</sup> 13 <sup>m</sup> 40 <sup>s</sup> .2	−69°25′37''	23.4	...	9.7±0.9
N 159W	05 <sup>h</sup> 40 <sup>m</sup> 01 <sup>s</sup> .5	−69°47′02''	57.0	45.6	20.8±2.2
N 167	05 <sup>h</sup> 44 <sup>m</sup> 17 <sup>s</sup> .6	−69°23′19''	19.8	15.5	5.6±1.1
N 214C	05 <sup>h</sup> 42 <sup>m</sup> 21 <sup>s</sup> .8	−71°20′33''	9.2	...	2.0±0.4
LIRL 648	05 <sup>h</sup> 14 <sup>m</sup> 07 <sup>s</sup> .0	−69°38′57''	13.1	...	6.7±1.2
<b>SMC</b>					
N 12	00 <sup>h</sup> 44 <sup>m</sup> 50 <sup>s</sup> .5	−73°22′33''	9.0	3.46	3.85±0.7
N 27	00 <sup>h</sup> 46 <sup>m</sup> 32 <sup>s</sup> .9	−73°21′50''	11.6	5.63	5.0±1.3
SMCB1#1	00 <sup>h</sup> 43 <sup>m</sup> 42 <sup>s</sup> .0	−73°35′10''	4.1	2.67	≤ 0.5
SMCB2#6	00 <sup>h</sup> 46 <sup>m</sup> 28 <sup>s</sup> .1	−73°34′10''	6.4	3.20	1.7±0.9
N 66	00 <sup>h</sup> 57 <sup>m</sup> 26 <sup>s</sup> .5	−72°26′36''	0.9	3.41 <sup>a</sup>	1.7±1.1
N 83	01 <sup>h</sup> 12 <sup>m</sup> 29 <sup>s</sup> .2	−73°32′40''	5.6	2.66	2.0±0.4

<sup>a</sup>Obtained from the  $^{13}\text{CO}$  ( $J = 1 \rightarrow 0$ ) map convolved to a HPBW=109'', assuming a  $^{12}\text{CO}/^{13}\text{CO}$  ratio  $\approx 11$ .

Note. — Nominal map center coordinates are indicated. Column 5 contains the  $^{12}\text{CO}$  ( $J = 1 \rightarrow 0$ ) integrated intensity in the ( $J = 4 \rightarrow 3$ ) beam for sources with ( $J = 1 \rightarrow 0$ ) maps.



Table 2. CO line intensity ratios of Magellanic Cloud Objects

Source	<sup>12</sup> CO Transition Ratios			<sup>12</sup> CO/ <sup>13</sup> CO Isotopic Ratios		References
	(2 → 1/1 → 0)	(3 → 2/1 → 0)	(4 → 3/1 → 0)	(1 → 0)	(2 → 1)	
<b>LMC</b>						
N 55A	...	...	0.51±0.17	11	...	1, 2
N 83A	...	...	1.58±0.52	9	...	1, 3
N 159W	0.90±0.25	0.9	0.46±0.15	9	5	1, 4, 5
N167	1.16±0.23	...	0.36±0.12	12	...	1, 6
<b>SMC</b>						
N 12	1.20±0.40	1.0	1.11±0.28	11	9	1, 7
N 27	0.95±0.35	0.75	0.89±0.30	17	11	1, 8, 9
SMCB1#1	0.72±0.12	0.4	≤0.2	11	13.5	1, 10, 11
SMCB2#6	...	...	0.53±0.28	...	...	1
N 66	1.30±0.35	1.0	0.50±0.32	11	7	1, 9, 10
N 83	1.19±0.31	...	0.56±0.22	10	9.5	1, 12

Note. — Ratios are determined from values in Table 1, and from previously published papers, mostly in the ESO Key Programme. References: (1) This Paper; (2) Israel et al. (1993); (3) Israel et al. (2003); (4) Johansson et al. (1998); (5) Bolatto et al. (2000); (6) Garay et al. (2002); (7) Chin et al. (1998); (8) Heikkilä et al. (1999); (9) Rubio et al. (1996); (10) Heikkilä (1998); (11) Rubio et al. (1993); (12) Bolatto et al. (2003).

determine the physical parameters best describing the conditions in the observed source. In principle, with two isotopes we need to measure five independent line intensities in order to fully determine the conditions of a single molecular gas component (i.e.  $T_k$ ,  $n(\text{H}_2)$ ,  $N(^{12}\text{CO})/dV$ ,  $N(^{13}\text{CO})/dV$  and a beam filling-factor). By assuming a fixed isotopical abundance  $[^{12}\text{CO}]/[^{13}\text{CO}] = 40$  (Johansson et al. 1994) we may decrease this requirement to four independent line intensities. As Table 2 shows, this minimum requirement is met by two out of nine LMC objects and five out of six SMC objects. The physical conditions of the remaining eight objects are, in principle, underdetermined.

More realistic, and consequently more complex, models of gas excitation that include more than one component require many more observations to be properly constrained. Full modelling of a two-component molecular cloud using two isotopes requires ten independent measurements, which again are reduced to eight by the introduction of a fixed isotopical abundance. As this is more than we have actually observed in any of the LMC or SMC clouds, it is clear that the solutions may not be unique. As long as the range of possible solutions is not excessive, however, they are still useful to constrain the physical parameters governing the observed emission.

We identified acceptable fits by searching a grid of model parameter combinations ( $10 \text{ K} \leq T_k \leq 150 \text{ K}$ ,  $10^2 \text{ cm}^{-3} \leq n(\text{H}_2) \leq 10^5 \text{ cm}^{-3}$ ,  $6 \times 10^{15} \text{ cm}^{-2} (\text{km s}^{-1})^{-1} \leq N(\text{CO})/dV \leq 3 \times 10^{18} \text{ cm}^{-2} (\text{km s}^{-1})^{-1}$ ) for model line ratios matching the observed values. Although errors in the line ratios increase the range of possible solutions, these ratios tend to define reasonably well-constrained regions of parameter space. The solutions are somewhat degenerate, as variations in the parameters may compensate one another. For instance, a simultaneous increase in kinetic temperature and decrease in  $\text{H}_2$  densities (or vice versa) yields similar line ratios (see § 3.2.3).

### 3.2. Single-component fits

#### 3.2.1. Objects with two measured intensities

For three objects (LMC-N 48, LMC-N 214C, and SMCB2#6) we only have intensities in the ( $J = 1 \rightarrow 0$ ) and ( $J = 4 \rightarrow 3$ ) transitions of  $^{12}\text{CO}$ . The parameters of these clouds are thus poorly constrained, and not summarized in a table. Assuming a single molecular gas component, we find for SMCB2#6 no effective constraints:  $T_k = 20\text{--}150 \text{ K}$ ,  $n(\text{H}_2) = 10^2\text{--}10^4 \text{ cm}^{-3}$ , and  $N(\text{CO})/dV = 10^{16}\text{--}10^{18} \text{ cm}^{-2} (\text{km s}^{-1})^{-1}$ . All  $^{12}\text{CO}$  transitions should be very optically thick. LMC-N 214C is slightly better determined: temperatures below 30 K are not allowed and densities appear high  $n(\text{H}_2) = 10^4\text{--}10^5 \text{ cm}^{-3}$ . The ( $J = 1 \rightarrow 0$ ) transition should not be very optically thick (although the higher transitions are) and its isotopic intensity ratio should be 10 – 20, as is in fact commonly observed in the LMC

(Israel et al. 2003). Finally, the high  $^{12}\text{CO}$  ( $J = 4 \rightarrow 3$ )/( $J = 1 \rightarrow 0$ ) ratio exhibited by LMC-N 48 are, in the single-component approximation, only consistent with low optical depths (isotopic intensity ratios 20 – 40), rather high densities  $n(\text{H}_2) = 10^4 - 10^5 \text{ cm}^{-3}$  and temperatures  $T_k = 60\text{--}150 \text{ K}$ , and gradients  $N(\text{CO})/dV = 10^{16} - 10^{17} \text{ cm}^{-2} (\text{km s}^{-1})^{-1}$ .

### 3.2.2. Objects with three measured intensities

For five objects, all in the LMC, (N 55, N 79, N 83A, N 113 and LIRL 648) we have measured  $^{13}\text{CO}$  ( $J = 1 \rightarrow 0$ ) intensities in addition to the  $^{12}\text{CO}$  ( $J = 1 \rightarrow 0$ ) and ( $J = 4 \rightarrow 3$ ) intensities. As is clear from the previous discussion, the molecular gas parameters are still underdetermined, but not fully unconstrained (Table 3). Both N 79 and N 113 fit very well to a hot and fairly dense model cloud with  $T_k = 100\text{--}150 \text{ K}$ ,  $n(\text{H}_2) = 3000 - 5000 \text{ cm}^{-3}$  and a gradient of about  $6 \times 10^{17} \text{ cm}^{-2} (\text{km s}^{-1})^{-1}$ . LIRL 648 is fit, but not very well, by a gas at the somewhat lower temperature of 60 K and the somewhat higher density of  $10^4 \text{ cm}^{-3}$ . The physical parameters of the molecular gas cloud associated with N 83A are inconsistent with the assumption of a single component. Only a very poor fit is obtained in the high-temperature, high-density, and high-velocity gradient limit.

### 3.2.3. Objects with four or more measured intensities

Seven objects have a sufficiently large number of measured line intensities to allow a full determination of physical parameters, assuming they can be properly described by a single molecular gas component. This appears indeed to be the case for SMCB1#1, where we find excellent agreement between the observed ratios and those of a model gas characterized by  $T_k = 50 \text{ K}$ ,  $n(\text{H}_2) = 700 \text{ cm}^{-3}$ ,  $N(\text{CO})/dV = 5 \times 10^{16} \text{ cm}^{-2} (\text{km s}^{-1})^{-1}$ . To fine-tune the solutions, as well as to gain insight into the various trade-offs, we have run a finer grid of models for this particular source. We summarize the best solutions for the temperature range  $T_k = 30\text{--}60 \text{ K}$  in Table 4. The overall best fit is achieved using a kinetic temperature  $T_k = 50 \text{ K}$ , and a density  $n(\text{H}_2) = 700 \text{ cm}^{-3}$ . At constant temperature, the uncertainty in density is about 20%. From the Table, it is also clear that we may allow for a similar temperature uncertainty of 20% if we simultaneously increase or decrease the density by 40%.

The good fit between model and observed line ratios is of particular significance because the solution is overdetermined with six independent intensity measurements. SMCB1#1 is a small and isolated molecular cloud in the SMC Bar, not associated with a star-forming

Table 3. Model physical parameters – single component fits

Source	Kinetic Temperature $T_k$ (K)	Volume Density $n(\text{H}_2)$ ( $\text{cm}^{-3}$ )	Column Density $N(\text{CO})/dV$ ( $\text{cm}^{-2}\text{km}^{-1} \text{ s}$ )
<b>LMC</b>			
N 55	30–60	$3 \times 10^3$	$1 \times 10^{17}$
N 79	100	$5 \times 10^3$	$6\text{-}10 \times 10^{17}$
N 113	150	$3 \times 10^3$	$6 \times 10^{17}$
N 159W	150	$10^3$	$3 \times 10^{17}$
LIRL 648	60	$10^4$	$3 \times 10^{17}$
<b>SMC</b>			
SMCB1#1	50	$7 \times 10^2$	$0.5 \times 10^{17}$

Table 4. Model fits for SMCB1#1

$T_{\text{kin}}$ (K)	$n(\text{H}_2)$ ( $\text{cm}^{-3}$ )	$N(\text{CO})/dV$ ( $\text{cm}^{-2} (\text{km s}^{-1})^{-1}$ )	$I^{12}\text{CO}/I^{13}\text{CO}$		$^{12}\text{CO}$ Rotational Ratio		
			( $J = 1 \rightarrow 0$ )	( $J = 2 \rightarrow 1$ )	(1-0/2-1)	(3-2/2-1)	(4-3/2-1)
<b>Observed constraints</b>							
...	...	...	11.2	13.5	1.4	0.6	$\leq 0.24$
<b>Modeling results</b>							
60	500	$6 \times 10^{16}$	10.4	12.0	1.41	0.56	0.23
50	600	$5 \times 10^{16}$	11.4	12.2	1.45	0.54	0.21
50	700	$5 \times 10^{16}$	12.0	12.2	1.43	0.56	0.23
50	800	$5 \times 10^{16}$	12.4	11.8	1.40	0.57	0.24
40	1100	$5 \times 10^{16}$	12.4	11.2	1.37	0.58	0.24
30	2000	$4 \times 10^{16}$	14.1	10.8	1.30	0.59	0.24

region (Rubio et al. 1993; Reach, et al. 2000; Rubio et al. 2004), thus a low density of  $\sim 700 \text{ cm}^{-3}$  is not necessarily surprising, although the kinetic temperature is higher than we would have expected for such a cloud in the Milky Way. Table 4, however, illustrates the difficulty in pinning down the physical conditions even in a simple cloud with a simple model.

The measured intensities of N 159-W can also be fit, albeit somewhat poorly, by a single hot ( $T_k = 150 \text{ K}$ ) and moderately dense component ( $n(\text{H}_2) = 1000 \text{ cm}^{-3}$ ). However, none of the other five objects have intensities consistent with a single component. Typically, a component fitting the observed  $^{12}\text{CO}$  line ratios would fail completely to explain the  $^{12}\text{CO}/^{13}\text{CO}$  isotopical ratios, indicating that in addition to a warm gas component the presence of a second cooler and dense component should be assumed. The lack of associated luminous objects probably explains the exceptionally homogeneous nature of SMCB1#1, required for such a well-determined single-component fit to be valid.

### 3.3. Dual-component fits

Since (with the exception of SMCB1#1 and perhaps N 159-W) *none* of the sources for which a lot of constraints are available allows a good fit with a single gas component, we suspect that the succesful single-component fits of the sources in Table 3 result primarily from insufficient information rather than from a simple physical structure. Attempts at more sophisticated modelling achieve little of value for most of these sources. The single exception is LMC-N 83A where only two observed ratios nevertheless conflict with every single component model tried. A dual component model yields acceptable but, not surprisingly, poorly constrained solutions (see Table 5). For all the other well-observed sources where single-component model fits failed, we have also constructed dual-component fits which are likewise listed in Table 5. This table shows that usually one of the two components component is reasonably well-determined, whereas the parameters of the other are generally less tightly constrained.

## 4. Summary and Conclusions

A general result of our survey is the detection of significant  $^{12}\text{CO}$  ( $J = 4 \rightarrow 3$ ) emission in most molecular peaks in the Magellanic Clouds. By itself this demonstrates the widespread occurrence of significant amounts of warm molecular gas, as tentatively suggested by Israel et al. (2003). Application of LVG model calculations show that molecular gas kinetic temperatures as high as  $T_{\text{kin}} = 100 - 300 \text{ K}$  frequently occur. Detailed analysis of the objects

for which multiple line ratios are available strongly suggests that the higher temperatures occur in cloud regions that are not very dense ( $n_{\text{H}_2} = 10^2 - 10^3 \text{ cm}^{-3}$ ), and that this gas is generally associated with colder (typically  $T_{\text{kin}} = 10 - 60 \text{ K}$ ) but much denser ( $n_{\text{H}_2} = 10^4 - 10^5 \text{ cm}^{-3}$ ) molecular gas. The simplified analysis possible in cases where fewer line ratios are available strongly suggests that the situation in those objects is similar. We note that recently reported observations of the N 44 complex in the LMC by Kim et al. (2004) show also the presence of strong  $^{12}\text{CO}$  ( $J = 4 \rightarrow 3$ ) emission, leading the authors to conclude the likely presence of very high densities ( $n_{\text{H}_2} \approx 10^5 \text{ cm}^{-3}$ ).

A few clouds are notable in our survey. Already mentioned is the case of SMCB1#1, a quiescent, compact molecular cloud devoid of any star forming activity. It appears to be essentially homogeneous and of modest density ( $n_{\text{H}_2} = 700 \text{ cm}^{-3}$ ), but is surprisingly warm ( $T_{\text{kin}} = 50 \text{ K}$ ). As there are no known embedded heating sources, this temperature must be maintained by the environment of the cloud, located in the south west region of the SMC Bar. The other two notable objects also occur in the SMC. N 12 is likewise located in the southern part of the Bar. Here, both the dense and relatively tenuous molecular phases appear to be surprisingly hot ( $T_{\text{kin}} = 150 \text{ K}$ ). In N 66, a very hot ( $T_{\text{kin}} = 300 \text{ K}$ ) and a cooler ( $T_{\text{kin}} = 40 \pm 20 \text{ K}$ ) phase coexist, *both* at a rather high density of the order of  $n_{\text{H}_2} = 10^4 \text{ cm}^{-3}$ . This particular molecular cloud is a relatively small remnant in a large and luminous star-forming complex (c.f., Rubio et al. 1996). It is almost certainly in an advanced stage of destructive processing; high densities and temperatures are consistent with such a situation (Rubio et al. 2000; Contursi et al. 2000).

Have we found signs of metallicity effects on the temperature equilibrium of the ISM in metal-poor environments? Given the measurement uncertainties and the dearth of comparable datasets on “normal” clouds in our own galaxy such finding cannot be asserted on the present measurements. It is suggestive, however, that high temperatures seem pervasive even in largely quiescent clouds such as SMCB1#1. This result should be taken with caution, as we suffer from a strong sample selection bias: the brightness of the optically thick  $^{12}\text{CO}$  ( $J = 1 \rightarrow 0$ ) transition is proportional to the source temperature and beam filling fraction, and we have pointed toward the brightest  $^{12}\text{CO}$  ( $J = 1 \rightarrow 0$ ) clouds. Thus it may not be surprising that our clouds are warm. Furthermore, studies of Galactic photodissociation regions (e.g., S 140, Draine & Bertoldi 1999; NGC 2023, Draine & Bertoldi 2000) find that  $\text{H}_2$  in star-forming clouds is frequently warmer than the theoretical expectation. Similarly, the intensities of the mid-J CO lines tend to be underpredicted by homogeneous PDR calculations (Hollenbach & Tielens 1999 and references therein). It is unclear whether these discrepancies are due to the presence of other heating mechanisms or to shortcomings in the models (e.g., Draine & Bertoldi 1999).

From the observational standpoint, a conclusive study of the effects of metallicity on gas temperature in the Magellanic Clouds must await the availability of more powerful submillimeter instruments observing the southern sky such as the Atacama Large Millimeter Array (ALMA), and the recently deployed single-dish telescopes: the Atacama Pathfinder Experiment (APEX) and the Atacama Submillimeter Telescope Experiment (ASTE).

We wish to thank the AST/RO group, and the anonymous referee. ADB wishes to thank D. Hollenbach for discussions on the subject of warm molecular gas, and for suggestions that helped improve this manuscript. ADB and CLM acknowledge support from NSF grants AST-0228963 and OPP-0126090 respectively.

## REFERENCES

- Bolatto A.D., Jackson J.M., Israel F.P., Zhang X., & Kim S., 2000 ApJ 545, 234
- Bolatto A.D., Leroy A., Israel F.P., Jackson J.M., 2003 ApJ 595, 167
- Chin Y.-N., Henkel C., Millar T. J., Whiteoak J. B. & Marx-Zimmer M. 1998 A&A 330, 901
- Contursi, A., et al. 2000, A&A, 362, 310
- Draine, B. T., & Bertoldi, F. 1999, in “The Universe as Seen by ISO”, eds. P. Cox & M. F. Kessler (ESA SP-427), 553
- Draine, B. T., & Bertoldi, F. 2000, in “Molecular Hydrogen in Space”, eds. F. Combes & G. Pineau de Forêts (Cambridge: Cambridge University Press), 131
- Garay G., Johansson L.E.B., Nyman L.-Å, et al. 2002 A&A 289, 977 (Paper VIII)
- Heikkilä A., 1998 Ph.D. thesis Chalmers Univ. (Sweden)
- Heikkilä A., Johansson L. E. B. & Olofsson H., 1999 A&A 344, 817
- Henize H., 1956 ApJS 2, 315
- Hollenbach, D., & Tielens, A.G.G.M. 1999, Reviews of Modern Physics, 71, 173
- Honingh, C. E., Delange, G., Dierichs, M. M. T. M., Schaeffer, H. H. A., Wezelman, J., Vandekuur, J., Degraauw, T., & Klapwijk, T. M. 1997, in “The Third International Symposium on Space Terahertz Technology”, 251
- Israel F.P., de Graauw Th., van de Stadt H., & de Vries C.P., 1986 ApJ 303, 186

- Israel F.P., Johansson L.E.B., Lequeux J., et al. 1993 A&A 276, 25 (Paper I)
- Israel F.P., Tacconi L.J., & Baas F., 1995 A&A 295, 599
- Israel F.P., Johansson L.E.B., Rubio M., et al. 2003 A&A 406, 817 (Paper X)
- Jansen D.J., 1995, Ph.D. thesis, University of Leiden (NL)
- Jansen D.J., van Dishoeck E.F. & Black J.H., 1994, A&A , 282, 605
- Johansson L.E.B., Olofsson H., Hjalmarson A., Gredel R., & Black J., 1994 A&A 291, 89
- Johansson L.E.B., Greve A., Booth R.S., et al. 1998 A&A 331, 857 (Paper VII)
- Kim S., Walsh W., Xiao K., 2004 ApJ 616, 865
- Le Bourlot, J., Pineau Des Forêts, G., Roueff, E., & Flower, D. R. 1993, A&A, 267, 233
- Leroy, A., Bolatto, A. D., Simon, J., & Blitz L. 2005, ApJ, in the press (astro-ph/0502302)
- Lisenfeld, U., & Ferrara, A. 1998, ApJ, 496, 145
- Madden, S. 2000, NewAR, 44, 249
- Reach, W. T., Boulanger, F., Contursi, A., Lequeux, J. 2000, A&A, 361, 895
- Rubio M., Lequeux J., Boulanger F., et al. 1993, A&A 271, 1
- Rubio M., Lequeux J., Boulanger F., et al. 1996, A&AS 118, 263
- Rubio, M., Contursi, A., Lequeux, J., Probst, R., Barbá, R., Boulanger, F., Cesarsky, D.,  
Maoli, R. 2000, A&A, 359, 1139
- Rubio, M., Boulanger, F., Rantakyro, F., Contursi, A. 2004, A&A, 425, L1
- Schieder, R., Tolls, V., & Winnewisser, G. 1989, Experimental Astronomy, 1, 101
- Stark, A. A., et al. 2001, PASP 113, 567
- Taylor, C. L., Kobulnicky, H. A., & Skillman, E. D. 1998, AJ, 116, 2746
- Walker, C. K., Kooi, J. W., Chant, M., Leduc, H. G., Schaffer, P. L., Carlstrom, J. E., &  
Phillips, T. G. 1992, International Journal of Infrared and Millimeter Waves, 13, 785
- Wolfire, M. G., Hollenbach, D., McKee, C. F., Tielens, A. G. G. M., & Bakes, E. L. O. 1995,  
ApJ 443, 152





Table 5. Model physical parameters – dual component fits

Source	‘Cold Dense’ Component			‘Hot Tenuous’ Component			Relative $J=2-1$ $^{12}\text{CO}$ Emission
	Kinetic Temperature $T_k$ (K)	Volume Density $n(\text{H}_2)$ ( $\text{cm}^{-3}$ )	Column Density $N(\text{CO})/dV$ ( $\text{cm}^{-2}\text{km}^{-1} \text{ s}$ )	Kinetic Temperature $T_k$ (K)	Volume Density $n(\text{H}_2)$ ( $\text{cm}^{-3}$ )	Column Density $N(\text{CO})/dV$ ( $\text{cm}^{-2}\text{km}^{-1} \text{ s}$ )	
<b>LMC</b>							
N 83A	10	$10^5$	$10 \times 10^{17}$	100	$10^5$	$3 \times 10^{17}$	3:2
	60	$10^5$	$1 \times 10^{17}$	150	$5-10 \times 10^2$	$6-10 \times 10^{17}$	4:1
	150	$10^5$	$3 \times 10^{17}$	150	$10^2$	$6-10 \times 10^{17}$	2:3
N 159W	20	$10^5$	$1 \times 10^{17}$	100	$10^2$	$1 \times 10^{17}$	1:1
N 167	20	$10^4$	$0.6 \times 10^{17}$	30–60	$1-10 \times 10^2$	$0.3-10 \times 10^{17}$	2:1
<b>SMC</b>							
N 12	150	$10^5$	$10 \times 10^{17}$	150	$1-5 \times 10^2$	$6 \times 10^{17}$	1:1
N 27	30	$10^5$	$0.6 \times 10^{17}$	60-100	$10^2$	$0.6 \times 10^{17}$	1:1
N 66	20–60	$10^4-10^5$	$6 \times 10^{17}$	300	$10^4$	$0.3 \times 10^{17}$	1:9
N 83	10–30	$10^4$	$1-2 \times 10^{17}$	100	$3 \times 10^3$	$0.3 \times 10^{17}$	1:8